Time domain and time spectral reduced order models for aeroelasticity

Fabrizio Di Donfrancesco, Antoine Placzek, Jean-Camille Chassaing

Time domain and time spectral reduced order models for aeroelasticity

F. Di Donfrancesco[1,2], A. Placzek[1] and J.-C. Chassaing[2]

[1] *DAAA/ONERA, Université Paris Saclay, F-92322 Châtillon, France, antoine.placzek@onera.fr*
[2] *Sorbonne Université, CNRS, Institut Jean Le Rond dAlembert, F-75005 Paris, France, jean-camille.chassaing@sorbonne-universite.fr*

Abstract

In this paper we address the construction of time and frequency domain Reduced Order Models for the Navier-Stokes equations. A classical basis obtained by the Proper Orthogonal Decomposition is used for the Galerkin projection of the governing equations and additional interpolation techniques based on the Discrete Empirical Interpolation Method are considered to evaluate efficiently the nonlinear terms. The applicability of this kind of ROMs for aeroelastic applications is first investigated in the time domain to reproduce the flow field around an oscillating cylinder at low Reynolds number. Then a second type of reduced order model dedicated to periodic flows is developed on the basis of the Time Spectral Method. Numerical tests demonstrate the potentiality of the proposed technique on the test case of an oscillating airfoil in subsonic and transonic regimes.

Keyword: Reduced Order Model, Proper Orthogonal Decomposition, Time Spectral Method, Discrete Empirical Interpolation Method

1 Introduction

Reduced-Order Models (ROMs) have been developed for decades in fluid dynamics as a way to decrease the cost of evaluating high fidelity solutions from a Full Order Model (FOM). Indeed, applications like parametric studies, optimization or control involving many queries to the FOM need fast evaluations which should be as accurate as possible. Projection based ROMs can be classically constructed using a basis built from a set of solutions snapshots whose meaningful content is extracted via a Proper Orthogonal Decomposition. Such projections lead to an explicit reduced operator in the linear or polynomial case (Hall et al. 1999; Placzek et al. 2011) but no explicit form can be obtained in general for nonlinear operators.

Flow non-linearities however arise commonly in aeronautical applications because of shock interaction, flow separation,... but also because of aeroelastic phenomena involving for example limit-cycle oscillations. High fidelity FOMs are therefore required to determine accurately the flow field but the large number of degrees of freedom involved in such models leads to unaffordable computational costs whose reduction represents one of the main motivation of this work. The projection based ROMs lacks efficiency when non-linearities are involved since in the general case the non-linear term has to be evaluated at the FOM level for each iteration.

To tackle this problem, the solution considered in the present paper is first to approximate the non-linear residual term using masked projection approaches like the Discrete Empirical Interpolation Method and its variants (Chaturantabut et al. 2010; Drmač et al. 2016). The non-linear term is thus interpolated (or fitted) on a small set of judiciously selected mesh points using an additional Proper Orthogonal Decomposition (POD) basis for the residual term. Interpolation techniques that preserve the basis structure are then implemented to update the basis content for new parameter values. An alternative solution proposed by Thomas et al. 2010 is to derive a Taylor series expansion of the reduced non-linear residual FOM solver which solves Euler or Navier-Stokes equations with the Time Spectral Method (TSM) (Hall et al. 2002; Gopinath et al. 2005). The resulting reduced operators are evaluated with automatic differentiation tools.

In the context of aeroelasticity, the FOM considered in the present paper is based on the Arbitrary Lagrangian Eulerian (ALE) formulation (Donea et al. 2004) and the problem of mesh deformation has to be taken into consideration, also at the ROM level. Following Anttonen et al. 2003 the POD basis for the snapshots of the solution and residual term can still be computed without explicitly taking care of the mesh deformation: the resulting POD modes are thus associated to the mesh connectivities in an "index" based framework and their usual spatial correlation meaning is no longer obvious. The mesh deformation is then taken into account in the approximated non-linear residual term of the ROM where the metric is updated with respect to the structural motion. This type of POD modes have been successfully used by Freno et al. 2014 in the time domain to address subsonic and transonic flows around airfoils subject to forced oscillations but the nonlinear term was treated at the FOM level. Other formulations considering a change of reference frame or small perturbations (Placzek et al. 2011; Bourguet et al. 2011) or the use of fictitious domains (Liberge et al. 2010) to keep the spatial correlations of the POD modes have also been derived for fluid-structure interaction problems.

The present methodology developed by Di Donfrancesco 2019 is first applied to build a ROM in the time domain on an apparently simple test case to highlight the difficulties of such time-domain ROMs to provide stable solutions on long term when masked projection approches are used to approximate the non-linear term. The TSM formulation of the ROM is investigated on the same test case and show better robustness even with respect to parameter changes. The long term stability of the solution is no longer a problem since a periodic solution is sought.

2 Governing equations for the full and reduced order models

2.1 Full Order Model in the time domain

The high fidelity FOM considered in the present paper is defined by the compressible Navier-Stokes equations. The ALE formulation is required to deal with aeroelastic problems involving possibly a non inertial and deformable spatial domain. Once discretized with hexahedral Finite Volumes, the semi-discrete form of the equations for a control cell $\Omega_i(t)$ reads:

$$\frac{\mathrm{d}}{\mathrm{d}t}(\mathcal{V}(\Omega_i)\mathbf{w}_i) = -\sum_{j=1}^{6} \mathbf{F}_i(\mathbf{w}_i, \mathbf{w}_j, \mathbf{s}_i)\,\mathbf{n}_j + \mathcal{V}(\Omega_i)\mathbf{T}_i = -\mathbf{R}_i(\mathbf{w}_i, \mathbf{w}_j, \mathbf{s}_i) \tag{1}$$

where $\mathbf{w}_i = [\rho_i, (\rho\mathbf{u})_i, (\rho e)_i]$ is the vector of the numerical approximation of the conservative variables in the control cell $\Omega_i(t)$ and $\mathbf{w}_j$ with $j \neq i$ is the approximation in neighbor control

cells involved in the spatial discretization scheme used to define the numerical fluxes $\mathbf{F}_i$ through the cell faces with normals $\mathbf{n}_j$. The ALE formulation introduces the mesh grid velocity $\mathbf{s}_i$ to take into account the grid deformation and the source term $\mathbf{T}_i$ may include additional terms due to a change of reference frame or some particular boundary conditions.

The spatial domain discretization $\Omega = \bigcup_{i=1}^{N} \Omega_i$ usually involves a large number of control cells N. The collection of the vectors of conservative variables $\mathbf{w}_i$ in each control cell may be assembled in a single vector $\mathbf{W} \in \mathbb{R}^{N_v}$ with $N_v = N \cdot n_v$ and n_v the number of conservative variables. The semi-discrete Navier-Stokes equations may then be formally written as an initial value problem defined by the nonlinear system of equations $\mathrm{d}/\mathrm{d}t(\boldsymbol{\mathcal{V}}\mathbf{W}) = \widetilde{\mathbf{R}}(\mathbf{W}, \mathbf{S})$ or similarly:

$$\frac{\mathrm{d}\mathbf{W}}{\mathrm{d}t} = \frac{\widetilde{\mathbf{R}}(\mathbf{W}, \mathbf{S})}{\boldsymbol{\mathcal{V}}} - \frac{\mathrm{d}\boldsymbol{\mathcal{V}}}{\mathrm{d}t}\frac{\mathbf{W}}{\boldsymbol{\mathcal{V}}} = \mathbf{R}(\mathbf{W}, \mathbf{S}) \tag{2}$$

with $\boldsymbol{\mathcal{V}}$ a diagonal matrix with all the control cell volumes $\mathcal{V}(\Omega_i)$ and $\mathbf{S}$ a vector containing all the mesh grid velocities $\mathbf{s}_i$. The previous equations are solved in the time domain with a high-order finite volume code (Chassaing et al. 2013) and will serve in the following as a basis to build the ROM and as a numerical reference to compare results from the ROM.

2.2 Projection based Reduced Order Model in the time domain

The first step of construction of the ROM consists in looking for an approximation of the conservative field $\mathbf{W}$ as the sum of a base solution $\mathbf{W_b}$ and a linear combination of appropriate spatial modes gathered in a basis $\boldsymbol{\Phi}$:

$$\mathbf{W}(t) \approx \mathbf{W}_b + \boldsymbol{\Phi}\,\mathbf{a}(t) \tag{3}$$

In this work, the spatial modes are computed with the Proper Orthogonal Decomposition (POD) of a set of representative solutions, or "snapshots", of the FOM. The POD is indeed the most widely used approximation basis for fluid dynamics reduced-order modeling because of its optimal properties in a certain sense and its straightforward computation with the Singular Value Decomposition (SVD).

Assuming that the snapshots are centered with respect to a base solution $\mathbf{W}_b$ (steady, time-averaged or initial solution for example) and collected in a matrix $\boldsymbol{\mathcal{W}}_b = [\mathbf{W}(t_1) - \mathbf{W}_b, \dots, \mathbf{W}(t_{N_t}) - \mathbf{W}_b] \in \mathbb{R}^{N_v \times N_t}$ with N_t the number of collected snapshots, the set of snapshot may be decomposed with the SVD as:

$$\boldsymbol{\mathcal{W}}_b = \boldsymbol{\Phi}\,\boldsymbol{\Sigma}\,\mathbf{V}^{\mathsf{T}} = \boldsymbol{\Phi}\,\mathbf{A} \tag{4}$$

where the matrix $\boldsymbol{\Phi} \in \mathbb{R}^{N_v \times N_r}$ is an orthonormal matrix containing the left singular vectors corresponding to the POD mode vectors, with $N_r = \mathrm{rank}(\boldsymbol{\mathcal{W}}_b) \leq \min(N_v, N_t)$. The diagonal matrix $\boldsymbol{\Sigma} \in \mathbb{R}^{N_r \times N_r}$ contains the singular values of $\boldsymbol{\mathcal{W}}_b$ listed in order of decreasing magnitude. Finally the matrix $\mathbf{V} \in \mathbb{R}^{N_t \times N_r}$ contains right singular vectors and the product $\mathbf{A} = \boldsymbol{\Sigma}\,\mathbf{V}^{\mathsf{T}}$ may be viewed as coordinates associated to the POD modes so that a snapshot from the set $\boldsymbol{\mathcal{W}}_b$ can be recomputed exactly as $\mathbf{W}(t_i) = \mathbf{W}_b + \boldsymbol{\Phi}\mathbf{a}(t_i)$ with $\mathbf{a}(t_i) \in \mathbb{R}^{N_r}$ the i-th column of $\mathbf{A}$. The previous expression has finally the expected form of Eq. (3).

In the first step of reduction, only the first POD modes are kept in the basis $\boldsymbol{\Phi}$ since they contain most of the data to approximate the snapshots. A common measure of the basis

truncation is given by the relative information content defined by $E_{N_q} = \sum_{i=1}^{N_q} \sigma_i^2 / \sum_{i=1}^{N_r} \sigma_i^2$ with $N_q \leq N_r$. In the second step of reduction, the snapshots approximation Eq. (3) with the truncated basis $\mathbf{\Phi} = [\phi_1, \dots, \phi_{N_q}]$ with $N_q \ll N_v$ is substituted in the FOM Eq. (2) and the Galerkin projection leads to the reduced set of N_q equations for the modal coordinate vector $\mathbf{a}$:

$$\frac{\mathrm{d}\mathbf{a}(t)}{\mathrm{d}t} = \mathbf{\Phi}^\mathsf{T} \mathbf{R}\left(\mathbf{W_b} + \mathbf{\Phi}\,\mathbf{a}(t), \mathbf{S}\right) \tag{5}$$

The previous system of equations is a small dynamical system whose solution is the modal coordinate vector $\mathbf{a}$ which, combined to the POD basis $\mathbf{\Phi}$, provides the full flow field vector $\mathbf{W}$ any time instant t, possibly not included in the snapshots database $\mathcal{W}_b$. The reduced order model should also be able to provide a solution for other parameter values typical of the studied system provided that the spatial basis is updated.

The residual term $\mathbf{R}$ for the compressible Navier-Stokes equations is non-linear and cannot be expressed explicitly in terms of the coordinates $\mathbf{a}(t)$ unless specific approximations are introduced. Without any additional work, the evaluation of this term at each time step has to be performed at the FOM level but the gain in computational time, if any, is very limited since numerical operations are performed on large vectors of dimension N_v. To tackle this issue, the non-linear term may be approximated in the same way as the snapshots:

$$\mathbf{R}(\mathbf{W}(t)) \approx \mathbf{R}(\mathbf{W}_b) + \mathbf{\Psi}\,\mathbf{c}(t) \tag{6}$$

where the matrix $\mathbf{\Psi} \in \mathbb{R}^{N_v \times N_p}$ is obtained from a POD of the set of residual snapshots $\mathcal{R}_b = [\mathbf{R}(\mathbf{W}(t_1)) - \mathbf{R}(\mathbf{W}_b), \dots, \mathbf{R}(\mathbf{W}(N_t)) - \mathbf{R}(\mathbf{W}_b)]$ and the vector $\mathbf{c}(t) \in \mathbb{R}^{N_p}$ gathers the coordinates associated to the POD modes of the residual term. The evaluation of this vector from the FOM residual with $\mathbf{c}(t) \approx \mathbf{\Psi}^\mathsf{T}[\mathbf{R}(\mathbf{W}(t)) - \mathbf{R}(\mathbf{W}_b)]$ would still involve costly operations sizing with N_v. We thus resort to masked projection techniques like the Discrete Empirical Interpolation Method (DEIM) (Chaturantabut et al. 2010) or its QDEIM variant (Drmač et al. 2016) to evaluate the unsteady term of the residual only on a small subset $N_f \ll N_v$ of control cells. The masked projection matrix $\mathbf{P} = [\mathbf{e}_{\wp_1}, \dots, \mathbf{e}_{\wp_{N_f}}] \in \mathbb{R}^{N_v \times N_f}$ with $\mathbf{e}_{\wp_i}$ the i-th column of the identity matrix of size N_v corresponds to the cell selection operation and has to be expanded to neighbor cells so that the residual term can be evaluated locally as $\mathbf{P}^\mathsf{T}\mathbf{R}(\mathbf{W}) = \mathbf{R_P}(\widetilde{\mathbf{P}}^\mathsf{T}\mathbf{W})$ where $\mathbf{R_P}$ is the residual operator evaluated only in the N_f cells and $\widetilde{\mathbf{P}} \in \mathbb{R}^{N_v \times (N_f + N_s)}$ is the expanded masked matrix with N_s the number of required neighbor cells depending on the spatial discretization scheme. The application of the masked matrix to Eq. (6) then provides the approximation $\mathbf{c}(t) \approx \mathbf{\Theta}[\mathbf{R_P}(\widetilde{\mathbf{P}}^\mathsf{T}\mathbf{W}(t)) - \mathbf{P}^\mathsf{T}\mathbf{R}(\mathbf{W}_b)]$ for the modal coordinates with the matrix $\mathbf{\Theta}$ depending on the invertibility of the matrix $\mathbf{P}^\mathsf{T}\mathbf{\Psi}$:

$$\mathbf{\Theta} = \begin{cases} (\mathbf{P}^\mathsf{T}\mathbf{\Psi})^{-1} & \text{if } N_f = N_p \\ (\mathbf{\Psi}^\mathsf{T}\mathbf{P}\mathbf{P}^\mathsf{T}\mathbf{\Psi})^{-1}\mathbf{\Psi}^\mathsf{T}\mathbf{P} & \text{if } N_f > N_p \end{cases} \tag{7}$$

These usual (Q)DEIM approximations provide as many interpolation points as the number of residual POD modes ($N_f = N_p$), but oversampling ($N_f > N_p$) is sometimes beneficial to improve the accuracy as sucessfully shown by Di Donfrancesco 2019 using a Block QDEIM approach. Finally the ROM with the approximation of the non-linear term is obtained after the substitution of the residual term approximation Eq. (6) in Eq. (5) and the replacement of the modal coordinate $\mathbf{c}$ by its approximation with the masked projection and reads:

$$\frac{\mathrm{d}\mathbf{a}(t)}{\mathrm{d}t} = \mathbf{\Phi}^\mathsf{T}(\mathbf{I} - \mathbf{\Psi}\mathbf{\Theta}\mathbf{P}^\mathsf{T})\,\mathbf{R}(\mathbf{W}_b) + \mathbf{\Phi}^\mathsf{T}\mathbf{\Psi}\mathbf{\Theta}\mathbf{R_P}(\widetilde{\mathbf{P}}^\mathsf{T}(\mathbf{W_b} + \mathbf{\Phi}\,\mathbf{a}(t))) \tag{8}$$

2.3 Full Order Model formulated with the Time Spectral Method

Provided that the FOM solution is periodic with period $T = 2\pi/\omega$, the conservative field vector and the residual term may be approximated by their truncated Fourier series $\mathbf{W} \approx \sum_{k=-N_h}^{N_h} \widehat{\mathbf{W}}_k e^{\jmath k\omega t}$ and $\mathbf{R} \approx \sum_{k=-N_h}^{N_h} \widehat{\mathbf{R}}_k e^{\jmath k\omega t}$ with $\tilde{N}_h = 2N_h + 1$ coefficients. The Fourier coefficients $\widehat{\mathbf{W}}_k$ are associated to their temporal counterpart $\mathbf{W}(t_n)$ at different time instants via the Discrete Fourier Transform (DFT). The matrix of Fourier coefficients $\widehat{\boldsymbol{\mathcal{W}}} = [\widehat{\mathbf{W}}_{-N_h}, \dots, \widehat{\mathbf{W}}_{+N_h}]^\mathsf{T}$ is then derived from the temporal snapshots matrix $\boldsymbol{\mathcal{W}} = [\mathbf{W}(t_0), \dots, \mathbf{W}(t_{2N_h})]^\mathsf{T}$ with $t_n = nT/\tilde{N}_h$ via the weight matrix $\boldsymbol{\mathcal{E}}$ with general term $\mathcal{E}_{k,n} = \tilde{N}_h^{-1} e^{-2\jmath\pi kn/\tilde{N}_h}$ such that $\widehat{\boldsymbol{\mathcal{W}}} = \boldsymbol{\mathcal{E}}\boldsymbol{\mathcal{W}}$.

Since the Fourier basis with the exponential functions $\{e^{\jmath k\omega t}\}_{k=-N_h}^{N_h}$ is orthonormal, the truncated Fourier series of eq.(2) with N_h harmonics reduces to a set of $\tilde{N}_h$ equations which can be recast in the condensed matrix form: $\boldsymbol{\mathcal{D}}\widehat{\boldsymbol{\mathcal{W}}} = \widehat{\boldsymbol{\mathcal{R}}}(\boldsymbol{\mathcal{W}})$ with $\widehat{\boldsymbol{\mathcal{R}}}$ the matrix of Fourier coefficients for the residual term and $\boldsymbol{\mathcal{D}} = \mathrm{diag}(-\jmath\omega N_h, \dots, \jmath\omega N_h)$. The explicit derivation of the residual term with respect to the Fourier coefficients of the conservative variables $\widehat{\boldsymbol{\mathcal{R}}}(\boldsymbol{\mathcal{E}}^{-1}\widehat{\boldsymbol{\mathcal{W}}})$ may be cumbersome and the Time Spectral Method (Hall et al. 2002; Gopinath et al. 2005) recasts the problem in the time domain while keeping the truncated Fourier approximation for the conservative variables and the residual term. The equations then read $\boldsymbol{\mathcal{E}}^{-1}\boldsymbol{\mathcal{D}}\boldsymbol{\mathcal{E}}\boldsymbol{\mathcal{W}} = \boldsymbol{\mathcal{R}}(\boldsymbol{\mathcal{W}})$ where the left hand size is the spectral approximation of the time derivative operator with N_h harmonics. For each time instant, the spectral derivative operator which couples all the time instants may be expressed analytically (Gopinath et al. 2005) and the problem is solved with a pseudo-time stepping technique. In practice the TSM problem uses the residual vector and Jacobian matrix provided by ONERA's code *elsA* (Cambier et al. 2013; Blondeau et al. 2019):

$$\frac{\mathrm{d}\mathbf{W}(t_n)}{\mathrm{d}\tau} = D_t(\mathbf{W}(t_n)) - \mathbf{R}(\mathbf{W}(t_n)) = \mathbf{R}_{\mathrm{TSM}}(\mathbf{W}(t_n)) \quad \forall\, 0 \leq n < 2N_h + 1 \tag{9}$$

2.4 Projection based Reduced Order Model with the Time Spectral Method

In this section we introduce a Reduced Order Time Spectral Method (ROTSM) which reduces the computational cost and exhibits better convergence properties than the Full Order TSM (FOTSM). The snapshot database $\boldsymbol{\mathcal{W}}$ contains the different time instants and is approximated by a POD such that $\mathbf{W}(t_n) = \boldsymbol{\Phi}\mathbf{a}(t_n)$. Note that unlike the POD for the time domain Eq. (3), the snapshots are not centered around a base field and the basis is not truncated since the rank $N_r = \tilde{N}_h$ is already very small.

The residual $\mathbf{R}_{\mathrm{TSM}}$ in Eq. (9) can be rewritten with the POD for each time instant as $D_t(\boldsymbol{\Phi})\mathbf{a}(t_n) - \mathbf{R}(\boldsymbol{\Phi}\mathbf{a}(t_n))$ and depends on the vector $\mathbf{a} = [\mathbf{a}(t_0), \dots, \mathbf{a}(t_{2N_h})]$ since the evaluation of the derivative operator couples all the time instants. The $\tilde{N}_h$ equations for all time instants can be gathered in a single residual term $\boldsymbol{\mathcal{R}}_{\mathrm{TSM}}(\mathbf{a})$ and the system of equations is solved iteratively with Newton's method so that the increment $\Delta\mathbf{a}^{(m)}$ for the iteration m is given by:

$$\boldsymbol{\mathcal{J}}^{(m)}\Delta\mathbf{a}^{(m)} = -\boldsymbol{\mathcal{R}}_{\mathrm{TSM}}(\mathbf{a}^{(m)}) \tag{10}$$

with $\boldsymbol{\mathcal{J}}^{(m)} = \mathbf{J}^{(m)}\boldsymbol{\Phi}_D$, where the residual Jacobian is $\mathbf{J}_{i,j}^{(m)} = \partial\mathbf{R}_{\mathrm{TSM}}(\boldsymbol{\Phi}\mathbf{a}(t_i))/\partial(\boldsymbol{\Phi}\mathbf{a}(t_j))$ and $\boldsymbol{\Phi}_D$ is a block diagonal matrix with the POD basis, see (Di Donfrancesco 2019) for further details. The system Eq. (11) can finally be projected on the basis $\boldsymbol{\Phi}_D$ to obtain a very small

system of $\tilde{N}_h$ equations such that:

$$\left[\boldsymbol{\Phi}_D^{\mathsf{T}}\boldsymbol{\mathcal{J}}^{(m)}\right]\Delta\mathbf{a}^{(m)} = -\boldsymbol{\Phi}_D^{\mathsf{T}}\boldsymbol{\mathcal{R}}_{\mathrm{TSM}}(\mathbf{a}^{(m)}) \tag{11}$$

This last formulation is apparently attractive since the projected Jacobian and residual terms in Eq. (11) scale with $\tilde{N}_h$. However since the residual is nonlinear, it has to be first evaluated with the FOTSM and then projected, unless an additional approximation is introduced. The masked projection approaches used in the time domain could as well be considered to approximate the residual and the Jacobian of the ROTSM and further work has to be conducted to evaluate this approach. Note that although Eq. (10) is not projected, the computational cost for the resolution is still reduced since the Jacobian $\boldsymbol{\mathcal{J}}$ has only $\tilde{N}_h^2$ columns instead of $\tilde{N}_h \cdot N_v$ with the FOTSM. The convergence is also accelerated with respect to the FOM since the initial guess for $\mathbf{a}$ comes from the projection of an initial field $\mathbf{W}_0$ on the POD basis which is presumably a good representation of the solution.

2.5 POD basis adaptation for parametrized ROMs

The ROMs detailed in previous sections have to provide accurate solutions in a certain range of a parameter λ. A global POD basis can be computed from a set of snapshots including different time instants and different parameter values: $\boldsymbol{\mathcal{W}} = [\mathbf{W}(t_1, \lambda_1), \dots, \mathbf{W}(t_M, \lambda_P)]$. However the resulting POD modes are no longer optimal for any parameter value and many modes have to be considered since the first modes represent average fields common to all parameter values (Amsallem 2010; Di Donfrancesco 2019). Another solution is to compute several POD bases $\boldsymbol{\Phi}_{\lambda_p}$ from the snapshots sets $\boldsymbol{\mathcal{W}}_{\lambda_p} = [\mathbf{W}(t_1, \lambda_p), \dots, \mathbf{W}(t_M, \lambda_p)]$ for $p = 1, \dots, P$. In this case the POD bases are optimal for each parameter λ_p. Then the POD basis for a new parameter value $\lambda^\star \notin \Lambda = \{\lambda_p\}_{p=1}^P$ is interpolated on the tangent space of the Grassmann manifold associated to the set of POD bases (Amsallem 2010). Such a procedure has been successfully used by Freno et al. 2014 for example on similar aeroelastic problems. Once in the tangent space, the interpolation can be performed with any classical interpolation method and the interpolated point is then sent back to the Grassmann manifold to obtain a representative subspace for the new parameter value.

3 Numerical applications

3.1 Time domain ROM for the flow around an oscillating cylinder at low Reynolds number

The accuracy of the time domain ROM is investigated on the example of an oscillating cylinder in a laminar cross-flow at $\mathrm{Re} = 185$. The vertical motion of the cylinder is prescribed with the function $y(t) = A\sin(2\pi f t)$ and different values of the normalized amplitude $A_r = A/d$ and frequency $f_r = f/f_S$ with d the cylinder diameter and f_S the vortex shedding frequency are investigated by Di Donfrancesco 2019. Numerical simulations have been conducted for $(A_r, f_r) = (0.2, 0.8)$ and $(0.5, 1.2)$ where secondary frequencies are observed in the flow field.

The Navier-Stokes equations are solved first with the FOM on a deforming grid to generate a set a snapshots selected after the transient phase. The relative information content of the POD modes is plotted in Fig. 1a and the first POD modes for $(A_r, f_r) = (0.2, 0.8)$ are shown in Fig. 1b. The time integration of the ROM is performed with a 4 steps Runge-Kutta method

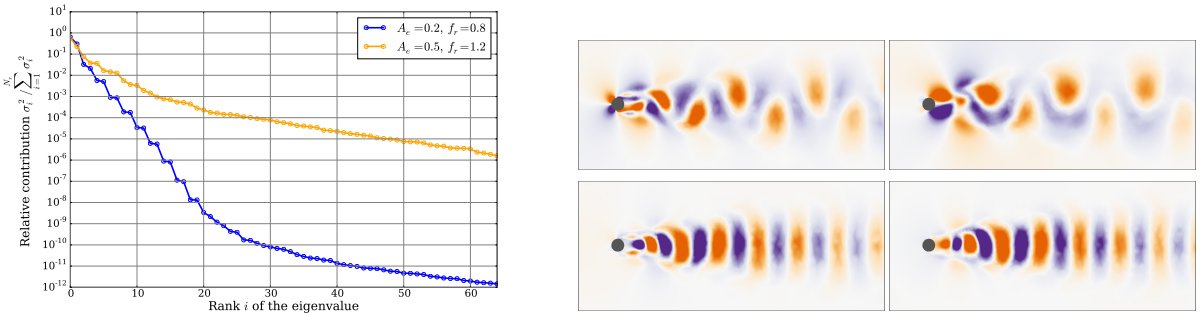

(a) Relative information content

(b) First four POD modes of density $(A_r, f_r) = (0.2, 0.8)$

Figure 1 – POD analysis of the oscillating cylinder at Re = 185.

for a single period of vortex shedding corresponding to the sampling time interval to compute the POD. Only $N_q = 12$ modes are sufficient to reproduce accurately the vortex shedding. Several tests have been conducted to check the robustness of the masked projection methods to approximate the nonlinear residual term.

The solution time histories of the first 3 modal coordinates $a_i(t)$ are plotted in Fig. 2a and 2b. Then the nonlinear term is approximated with the BQDEIM using N_p nonlinear residual POD modes and $N_f = b \cdot N_p$ interpolation points with $b = n_v = 4$ and $N_p = 14$ for $(A_r, f_r) = (0.2, 0.8)$ and $b = 20$ and $N_p = 40$ for $(A_r, f_r) = (0.5, 1.2)$. The results plotted in Fig. 2a and 2b are also satisfactory in both cases (see the difference plotted on the right axis) and the relative error for the density field at the last time instant plotted in Fig.2c is lower than 3% (less than 1.2% for $(A_r, f_r) = (0.2, 0.8)$).

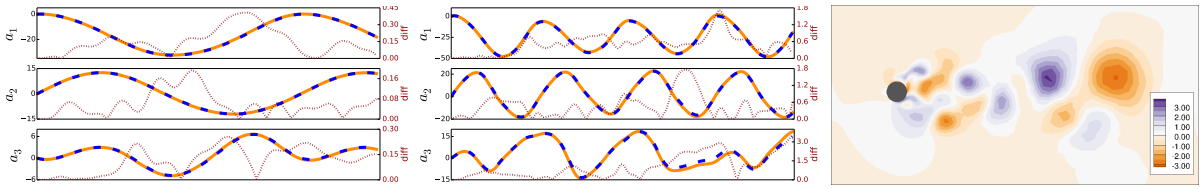

(a) $(A_r, f_r) = (0.2, 0.8)$.

(b) $(A_r, f_r) = (0.5, 1.2)$.

(c) Relative error on density field.

Figure 2 – Comparison of the first three modal coordinates time histories (– – FOM, — ROM) and density field error at Re = 185.

Additional test cases have been investigated in (Di Donfrancesco 2019) and a parametric investigation of the ROM with respect to the amplitude and frequency variation has also been conducted. Satisfactory results are obtained but the long term stability of the ROM is not always ensured for a new parameter value, even for this low Reynolds number test case. Note that the number of interpolation cells has to be increased up to 6% of the total number of cells in the second case $(A_r, f_r) = (0.5, 1.2)$ presented here. Special care has therefore to be taken for parametric investigations in order to ensure that a sufficient number of cells is used for the interpolation, whatever the value of the considered parameter.

3.2 ROTSM for the transonic flow around an oscillating airfoil

The second test case considered here is a transonic pitching NACA64A010 airfoil. Di Donfrancesco (2019) has shown that simulations with the time domain ROM fail to converge on

long term even in subsonic regime at Ma = 0.50 without masked projection and the robustness of the ROTSM is therefore demonstrated here. A reference simulation is first run for Ma = 0.796 with the Euler FOTSM implemented in (Blondeau et al. 2019) with $N_h = 1$ harmonic only The prescribed harmonic pitch motion is defined by $\alpha(t) = \alpha_0 + \hat{\alpha}\sin(2\pi f t)$ with $\alpha_0 = -0.22°$, $\hat{\alpha} = 1.01°$ and the frequency is set to $f = 34.4$ Hz.

The 3 TSM snapshots and the corresponding POD modes are plotted in Fig. 3. The POD basis is not truncated since the size is already very small. The convergence of the ROTSM is much faster than the one of the FOTSM since the initial uniform freestream solution is projected on the POD basis and provides a good guess for the modal coordinates. As shown in Fig. 4a the residual is close to the one of the FOM solution in about 20 iterations; it does not decrease further since the ROTSM solution (which is necessarily in the subspace spanned by the POD basis) can not be better than the FOTSM solution. The skin pressure is perfectly reproduced, as well as the lift and drag forces whose time history can be evaluated over a complete cycle of oscillation from its Fourier series as shown in Fig. 4b.

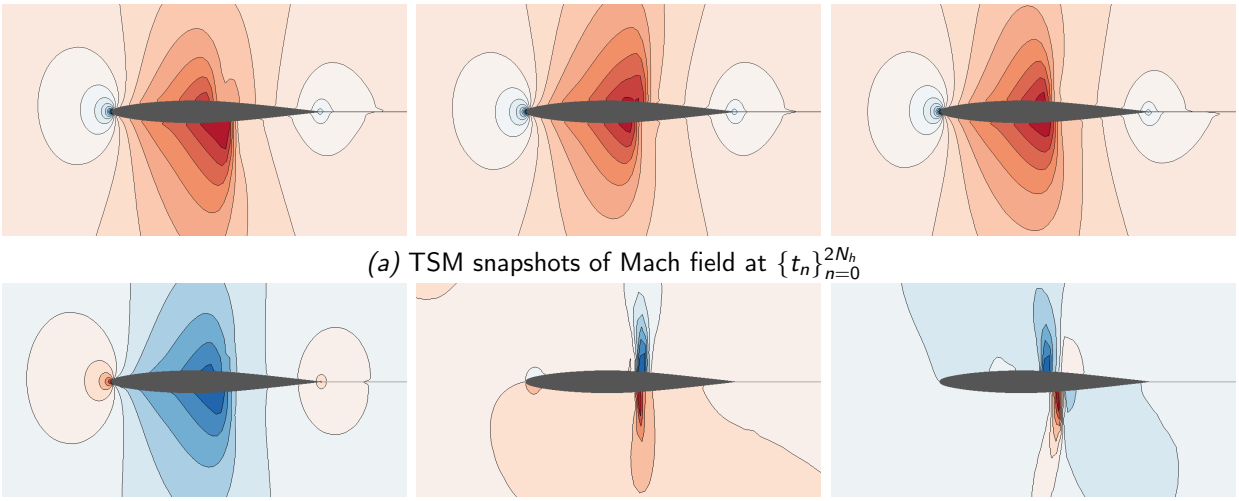

(a) TSM snapshots of Mach field at $\{t_n\}_{n=0}^{2N_h}$

(b) Proper orthogonal modes of density $\{\mathbf{\Phi}_i^{(\rho)}\}_{i=0}^{2N_h}$

Figure 3 – TSM snapshots and POD modes for the pitching airfoil at Ma = 0.796 with $N_h = 1$.

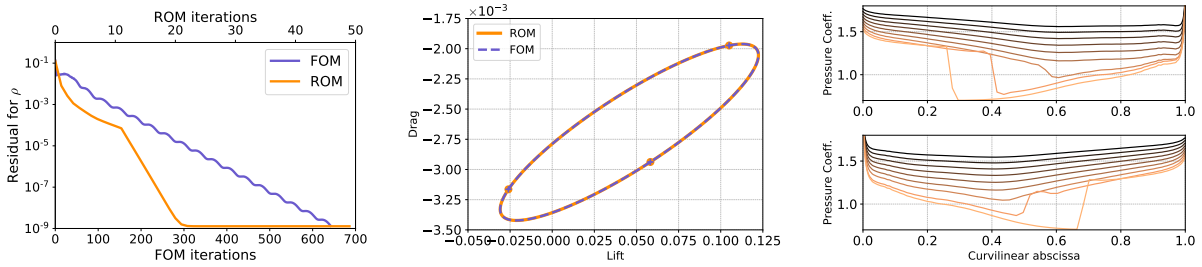

(a) Residual convergence for ρ *(b)* Lift vs Drag curve *(c)* Skin pressure variation

Figure 4 – ROTSM vs FOTSM results (a), (b) and database of skin pressure at t_0.

A database of reference simulations is then run at different Mach numbers Ma $\in [0.50; 0.84]$ from subsonic to transonic regime. The range of variation for the skin pressure is illustrated in Fig. 4c. A strong pressure gradient develops for Ma ≥ 0.76. A set of POD bases is first constructed with a regular sampling for Ma $\in \{0.52, 0.56, 0.60, 0.64, 0.68, 0.72, 0.76, 0.80, 0.84\}$

and the ROTSM is evaluated for new values of the Mach number $\mathrm{Ma}^\star \in \{0.58, 0.74, 0.79, 0.81\}$. Different interpolation methods on the tangent plane of the Grassmann manifold are compared in Tab. 1 for the average and maximal value of the relative error between the skin pressure computed by the ROTSM with respect to the FOTSM for the $2N_h + 1$ time instants.

Table 1 – Relative error in percentage for the skin pressure at all time instants between the FOM and the ROM for several interpolated Mach numbers with the first database.

	Mean error			Max. error		
	Linear	Spline	Lagrange	Linear	Spline	Lagrange
$\mathrm{Ma} = 0.58$	$8{,}15 \cdot 10^{-2}$	$4{,}06 \cdot 10^{-2}$	$1{,}07 \cdot 10^{-1}$	$8{,}38 \cdot 10^{+1}$	$4{,}58 \cdot 10^{+1}$	$2{,}18 \cdot 10^{+1}$
$\mathrm{Ma} = 0.74$	$2{,}95 \cdot 10^{-1}$	$4{,}30 \cdot 10^{-1}$	$2{,}39 \cdot 10^{-1}$	$5{,}50 \cdot 10^{+1}$	$1{,}09 \cdot 10^{+2}$	$5{,}00 \cdot 10^{+1}$
$\mathrm{Ma} = 0.79$	$7{,}29 \cdot 10^{-1}$	$6{,}70 \cdot 10^{-1}$	$7{,}59 \cdot 10^{-1}$	$1{,}78 \cdot 10^{+2}$	$1{,}59 \cdot 10^{+2}$	$2{,}10 \cdot 10^{+2}$
$\mathrm{Ma} = 0.81$	$7{,}55 \cdot 10^{-1}$	$8{,}21 \cdot 10^{-1}$	$1{,}71 \cdot 10^{+0}$	$1{,}79 \cdot 10^{+2}$	$2{,}94 \cdot 10^{+2}$	$8{,}97 \cdot 10^{+2}$

The relative mean error for the airfoil skin pressure is overall under 1% and increases with the Mach number. The maximal relative error is however much higher and increases significantly when the flow becomes transonic. The spline or Lagrange interpolation methods provide accurate results in subsonic regime but should be avoided when the flow becomes transonic because spurious oscillations in the interpolation lead to inaccurate results.

A second database for $\mathrm{Ma} \in \{0.50, .6, .70, .74, .76, 0.77, .78, .8, .82, .84\}$ is considered with a finer sampling in the transonic regime and less points in the subsonic one. Results in Table 2 indicate that the error can be substantially descreased in the transonic regime for $\mathrm{Ma} = 0.79$ and 0.81 but the integration sometimes fails with Lagrange interpolation. The error in the subsonic regime is larger than with the first database since the sampling is now coarser. Accurate results in subsonic and transonic regimes thus require a fine sampling in both regimes.

Table 2 – Relative error in percentage for the skin pressure at all time instants between the FOM and the ROM for several interpolated Mach numbers with the second database.

	Mean error			Max. error		
	Linear	Spline	Lagrange	Linear	Spline	Lagrange
$\mathrm{Ma} = 0.58$	$1{,}75 \cdot 10^{-1}$	$1{,}34 \cdot 10^{-1}$	—	$1{,}06 \cdot 10^{+2}$	$1{,}29 \cdot 10^{+2}$	—
$\mathrm{Ma} = 0.74$	$3{,}03 \cdot 10^{+0}$	$3{,}03 \cdot 10^{+0}$	$3{,}03 \cdot 10^{+0}$	$2{,}98 \cdot 10^{+2}$	$2{,}98 \cdot 10^{+2}$	$2{,}99 \cdot 10^{+2}$
$\mathrm{Ma} = 0.79$	$3{,}41 \cdot 10^{-1}$	$3{,}56 \cdot 10^{-1}$	$5{,}91 \cdot 10^{-1}$	$3{,}69 \cdot 10^{+1}$	$2{,}73 \cdot 10^{+1}$	$8{,}71 \cdot 10^{+1}$
$\mathrm{Ma} = 0.81$	$3{,}92 \cdot 10^{-1}$	$3{,}75 \cdot 10^{-1}$	—	$3{,}39 \cdot 10^{+1}$	$2{,}24 \cdot 10^{+1}$	—

4 Conclusions

ROMs in the time and frequency domains have been developed and used for aeroelastic applications in subsonic and transonic regime. For low Mach numbers, time domain ROMs with masked projection techniques provide accurate results, at least for short term time integration. An original BQDEIM approach was implemented to enable oversampling for the nonlinear term approximation and to improve the accuracy of the time domain ROM. When the Mach number increases, time domain ROMs lack robustness and the ROTSM formulation proved to be more robust. The parametric response has been investigated with several interpolations methods and database of POD bases. The database has to be refined to capture accurately the shock in the transonic regime and linear or spline interpolations are more stable than Lagrange interpolation.

References

Amsallem, D. (2010). "Interpolation on Manifolds of CFD-based Fluid and Structural Reduced-Order Models for On-Line Aeroelastic Predictions". PhD Thesis. Stanford University.

Anttonen, J., P. King, and P. Beran (2003). "POD-Based reduced-order models with deforming grids". *Mathematical and Computer Modelling* 38.1, pp. 41–62.

Blondeau, C. and C. Liauzun (2019). "A Modular Implementation of the Time Spectral Method for Aeroelastic Analysis and Optimization on Structured Meshes". *18th International Forum on Aeroelasticity and Structural Dynamics*. IFASD-2019-032. Savannah, Georgia, USA.

Bourguet, R., M. Braza, and A. Dervieux (2011). "Reduced-order modeling of transonic flows around an airfoil submitted to small deformations". *Journal of Computational Physics* 230.1.

Cambier, L., S. Heib, and S. Plot (2013). "The Onera elsA CFD software: Input from research and feedback from industry". *Mechanics & Industry* 14, pp. 159–174.

Chassaing, J.-C., X. Nogueira, and S. Khelladi (2013). "Moving Kriging reconstruction for high-order finite volume computation of compressible flows". *Computer Methods in Applied Mechanics and Engineering* 253, pp. 463–478.

Chaturantabut, S. and D. C. Sorensen (2010). "Nonlinear model Reduction via Discrete Empirical Interpolation". *SIAM Journal on Scientific Computing* 32.5, pp. 2737–64.

Di Donfrancesco, F. (2019). "Reduced Order Models for the Navier-Stokes equations for Aeroelasticity". PhD Thesis. Sorbonne University.

Donea, J. et al. (2004). "Encyclopedia of Computational Mechanics". Vol. 1: Fundamentals. John Wiley & Sons. Chap. 14: Arbitrary Lagrangian-Eulerian Methods, pp. 1–25.

Drmač, Z. and S. Gugercin (2016). "A New Selection Operator for the Discrete Empirical Interpolation Method - Improved a priori error bound and extensions". *SIAM Journal on Scientific Computing* 38.2.

Freno, B. A. and P. G. Cizmas (2014). "A proper orthogonal decomposition method for nonlinear flows with deforming meshes". *International Journal of Heat and Fluid Flow* 50.

Gopinath, A. and A. Jameson (2005). "Time Spectral Method for Periodic Unsteady Computations over Two- and Three- Dimensional Bodies". *43rd AIAA Aerospace Sciences Meeting and Exhibit*. Reno (NV).

Hall, K. C., J. P. Thomas, and E. H. Dowell (1999). "Reduced-Order Modelling of Unsteady Small-Disturbance Flows using a Frequency-Domain Proper Orthogonal Decomposition Technique". *37th Aerospace Sciences Meeting and Exhibit*. Reno (NV).

Hall, K. C., J. P. Thomas, and W. S. Clark (2002). "Computation of Unsteady Nonlinear Flows in Cascades Using a Harmonic Balance Technique". *AIAA Journal* 40.5, pp. 879–886.

Liberge, E. and A. Hamdouni (2010). "Reduced order modelling method via proper orthogonal decomposition (POD) for flow around an oscillating cylinder". *Journal of Fluids and Structures* 26.2, pp. 292–311.

Placzek, A., D.-M. Tran, and R. Ohayon (2011). "A nonlinear POD-Galerkin reduced-order model for compressible flows taking into account rigid body motions". *Computer Methods in Applied Mechanics and Engineering* 200.49-52, pp. 3497–14.

Thomas, J. P., E. H. Dowell, and K. C. Hall (2010). "Using Automatic Differentiation to Create a Nonlinear Reduced-Order-Model Aerodynamic Solver". *AIAA Journal* 48.1, pp. 19–24.